Correlated fission fragments emitted in the reaction of ^{16}O on ^{238}U at 20 MeV/nucleon

B. B. Back, K. L. Wolf, and A. C. Mignerey*
Chemistry Division, Argonne National Laboratory, Argonne, Illinois 60439

C. K. Gelbke and T. C. Awes
Cyclotron Laboratory, Michigan State University, East Lansing, Michigan 48824
and Lawrence Berkeley Laboratory, University of California, Berkeley, California 94720

H. Breuer and V. E. Viola, Jr.
Department of Chemistry, University of Maryland, College Park, Maryland 20742

P. Dyer
Cyclotron Laboratory, Michigan State University, East Lansing, Michigan 48824
(Received 21 April 1980)

The reactions induced by 315-MeV ^{16}O ions on ^{238}U have been studied by observing the folding angle between the two fission fragments resulting from the sequential fission decay of the target residue in coincidence with reaction products ranging from protons to ^{16}O ions. A kinematical analysis shows that the emission of light particles (p,d,t,α) plays an important role for both central and peripheral reactions. It is concluded that these particles, most likely, are emitted during the early stages of the reaction.

[NUCLEAR REACTIONS, FISSION $^{238}U(^{16}O,Xf)$, $X=p,d,t,\ldots,O$, $E=315$ MeV; measured $\sigma(E_x)$ and fission fragment folding angle distributions. Deduced missing momentum and fission fragment mass distributions.]

I. INTRODUCTION

Heavy ion reactions at bombarding energies below 10 MeV/nucleon have been studied intensively during recent years and the basic reaction mechanism is currently known in some detail.[1-4] The main contributions to the reaction cross section are compound nucleus formation and deep inelastic processes, both of which lead to subsequent particle decay, γ emission, or fission. Light particle spectra observed in these reactions can, to a remarkable degree, be accounted for by evaporation from thermally equilibrated, fully accelerated reaction partners or fission fragments.[5-7] However, there is evidence of some pre-equilibrium particle emission, mostly in connection with compound nucleus formation processes.[8-11] These effects are significantly more important, for both central and peripheral collisions, when the bombarding energy is increased to 20 MeV/nucleon.

In the present experiment we have studied the reactions resulting from the bombardment of a ^{238}U target with ^{16}O ions. We have chosen to investigate reactions on an actinide target (^{238}U) because of its low fission threshold.[12] As a consequence, fission is the dominant decay mode of the target residue and little selectivity is imposed on the reaction by requiring a fission coincidence. (Of course, a minimum inelasticity has to be required for the reaction to produce two fission fragments.) Detecting fission fragments in coincidence with other outgoing reaction products, therefore, imposes only a small bias on the reaction investigated and allows the study of rather global features of the reaction. Furthermore, by studying the fission decay in more detail we obtain information on the excitation energy of the target residues after the reaction has taken place. Thus, the folding angle between the resulting fission fragments is closely related to the amount of linear momentum transferred to the fissioning system[13,14] and the fission fragment mass distribution is, to some degree, a measure of the excitation energy of the fissioning nucleus. In this paper we will give a detailed description of the experimental setup and analysis, and discuss the results in terms of various models applicable to this energy regime. Some aspects of the present work have been published earlier in brief reports.[15,16]

II. EXPERIMENTAL ARRANGEMENT

Beams of 140 and 315 MeV ^{16}O ions were provided by the 88″ cyclotron at the Lawrence Berkeley Laboratory. The target consisted of 200 $\mu g/cm^2$ $^{238}UF_4$ material evaporated onto a 50 $\mu g/cm^2$ carbon foil. The detector arrangement is illustrated in Fig. 1. Two position sensitive solid state detectors (PSD) were placed on opposite sides of the beam axis, which allows for the simultaneous measurement of both fission fragment energies and laboratory angles. These detectors

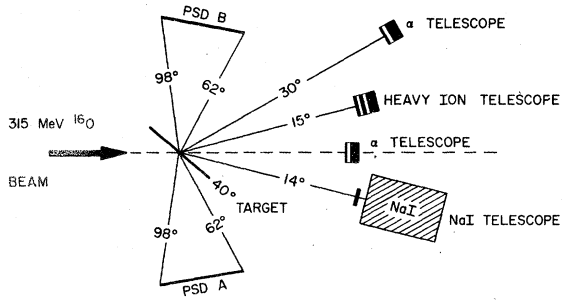

FIG. 1. Experimental geometry used in the present study.

were placed at a distance of 64 mm from the target. A heavy ion detector telescope consisting of two ΔE solid state detectors and one E detector of thicknesses 68, 95, and 5000 μm, respectively, was placed at $\theta = 15°$ relative to the beam axis subtending a solid angle of 7.5 msr. This telescope was used to detect projectile residues in coincidence with fission fragments. Energetic light particles (p, d, t, and α) were detected with a telescope consisting of a 375 μm thick surface barrier solid state detector placed in front of a 38 mm deep NaI scintillation detector. This telescope was placed at an angle $\theta_{\mathrm{NaI}} = -14°$ relative to the beam axis and subtended a solid angle of $\Omega_{\mathrm{NaI}} \simeq 7.6$ msr. In addition, alpha particles were measured with two solid state detector telescopes, consisting of 200–250 μm ΔE detectors and 5 mm thick E detectors, placed at the angles $\theta_{\alpha 1} = 30°$ in plane, and $\theta_{\alpha 2} = 26°$, $\phi_{\alpha 2} = 90°$ out of the reaction plane subtending solid angles of $\Omega_{\alpha 1} = 3.9$ msr and $\Omega_{\alpha 2} = 9.1$ msr, respectively.

Coincident events between two fission fragments (detected in the two position sensitive detectors) and projectile residues or light particles (detected in one of the four telescopes) were recorded, event by event, on magnetic tape using the LBL Modcomp computer system for subsequent off-line analysis.

The energy calibration for the two position sensitive detectors was obtained by recording the pulse height spectrum from ^{252}Cf spontaneous fission fragments and using the Schmitt[17] calibration procedure. A mask with 15 slits of 0.8 mm width was placed in front of the PSD's to obtain an accurate position calibration of the detectors using a ^{252}Cf fission source. In spite of the good position resolution of $\Delta S \leq 0.5$ mm it can be problematic to obtain an accurate scattering angle calibration. In order to achieve good efficiency for the detection of fission coincidences, the fission detectors have to be mounted close to the target. This close geometry renders the angle calibration quite sensitive to small uncertainties in the beam and target positions. In order to minimize the resulting systematic errors of the folding angle calibration we have performed a separate measurement of the inclusive fission-fission folding angle distributions at bombarding energies of 140 and 315 MeV with 4 different target orientations. These orientations were chosen as θ_t, $\pi - \theta_t$, $\pi + \theta_t$, and $2\pi - \theta_t$, where θ_t is the angle between the target plane and the beam axis. As shown in the Appendix, it is possible to measure and correct for the effects of the beam and target being off the center of the scattering chamber. Furthermore, it was required that the fission-fission folding angle observed in coincidence with inelastically scattered ^{16}O ions with $Q > -15$ MeV be consistent with a pure two body reaction followed by the fission decay of the target nucleus; i.e., we required that there were no unobserved particles emitted during the reaction, except fission neutrons, which do not affect the centroid of the folding angle distribution. With these corrections taken into account, it is estimated that the fission fragment folding angle is measured with an accuracy of $\Delta\theta_{AB} \lesssim 1°$. (See Appendix.)

The energy calibration of the NaI telescope was obtained by measuring the elastic scattering of protons and alpha particles at 21 and 79 MeV, respectively. The alpha particle and heavy ion telescopes were calibrated using ^{252}Cf, and ^{228}Th sources and a calibrated pulser input at the detector side of the preamplifiers. The time stability of the NaI crystal was monitored by observing the peak position of elastically scattered ^{16}O ions, which entered the detector through a hole of 1.6 mm diameter in the 0.8 mm thick Al cover foil that had been placed in front of the NaI telescope to cut down the elastic count rate in the detector.

III. DATA ANALYSIS

For the present experiment, 17 parameters were measured and recorded on magnetic tape. These parameters are the energy signals of all eleven detectors, the two position dependent signals for the position sensitive fission detectors, and the time to amplitude converter outputs that correspond to the time spectra measured between the fission detector PSD A and the four particle telescopes. In addition, we monitored the relative time spectra between the two fission detectors. Since these spectra contained only a negligible number of events corresponding to random coincidences (~10^4 real-to-random ratio), this parameter was not written on magnetic tape.

From the measured energy losses and energies, standard particle identification functions of the form

$$\mathrm{PI} = \mathrm{const}\,[(E+\Delta E)^x - E^x] \tag{1}$$

were generated for each telescope. Here, ΔE and E are the energy loss and the residual energy of the particle and x is a parameter that is optimized to give minimum energy dependence of the PI function (generally $x \approx 1.7$–1.8). With this method, mass and charge identification of the particles was obtained.

The coincidence data were analyzed off line by two different methods: First, the correlation between fission fragment folding angles in the laboratory system and energies of both light and heavy outgoing particles were established. This analysis contains no assumptions about the reaction mechanism and the results are thus model independent. Second, a more complete event by event analysis was performed in order to extract the amount of linear momentum transferred to the target residue prior to fission. In the present experiment, only two parameters—the energy and the outgoing direction—were determined for each fission fragment. The fragment masses were not measured and, consequently, the reconstruction of the kinematics of the fission reaction is not possible unless two more parameters for the fission fragments can be determined. In our analysis we have made specific assumptions about the sum mass of the primary fission fragments and about the target residue momentum component $P_R^{\perp}$ perpendicular to the beam axis. In the following paragraphs we give a detailed discussion of our kinematical analysis and the validity of our approximations.

We consider the fission decay of the recoiling nucleus as an isolated event; i.e., we assume a truly sequential fission process. Momentum conservation in the laboratory system then gives the following two equations:

$$P_R^{\parallel} = P_A \cos\theta_A + P_B \cos\theta_B \tag{2}$$

and

$$P_R^{\perp} = P_A \sin\theta_A - P_B \sin\theta_B\,, \tag{3}$$

where $P_R^{\parallel}$ and $P_R^{\perp}$ denote the parallel and perpendicular momentum components of the recoiling system with respect to the beam axis. The magnitude and angle of the momentum of fragment A with respect to the beam axis are denoted P_A and θ_A, respectively. A similar notation is adopted for the momentum of fragment B. Mass conservation during the fission decay can be expressed as

$$M_R = M_A + M_B\,, \tag{4}$$

where M_R, M_A, and M_B are the masses of the recoil nucleus and the primary fragments A and B, respectively.

The momenta of the primary fission fragments are given by

$$P_A = (2M_A E_A)^{1/2}\,, \tag{5a}$$

$$P_B = (2M_B E_B)^{1/2}\,, \tag{5b}$$

where E_A and E_B denote the primary fragment kinetic energies. (For the discussion of the corrections for neutron evaporation from the primary fragments, see below.) It is clear that two more equations are needed to determine the momentum of the target residue.

If the primary reaction between the projectile and target residue were a pure two body process we would have the additional relations

$$P_R^{\parallel} = P_1 - P_3^{\parallel}\,, \tag{6a}$$

$$P_R^{\perp} = -P_3^{\perp}\,, \tag{6b}$$

$$M_R = M_1 + M_2 - M_3\,, \tag{6c}$$

where the indices 1, 2, and 3 denote the projectile, the target, and the outgoing projectile residue, respectively. Since only two relations are needed to determine the kinematics unambiguously, we have measured one redundant parameter in this case, which can then be used to check on the assumption of a primary two body reaction.

In the general case, we are dealing with more than three particles in the exit channel, and Eqs. (6) are no longer fulfilled. If we denote the total mass and momentum of all undetected particles by the "missing momentum" P_m and the "missing mass" M_m, we have instead (see Fig. 2)

$$P_R^{\parallel} = P_1 - P_3^{\parallel} - P_m^{\parallel}\,, \tag{7a}$$

$$P_R^{\perp} = -P_3^{\perp} - P_m^{\perp}\,, \tag{7b}$$

$$M_R = M_1 + M_2 - M_3 - M_m\,. \tag{7c}$$

In the following we will show that the momentum components parallel to the beam axis, $P_R^{\parallel}$ and $P_m^{\parallel}$, are quite well determined by the present mea-

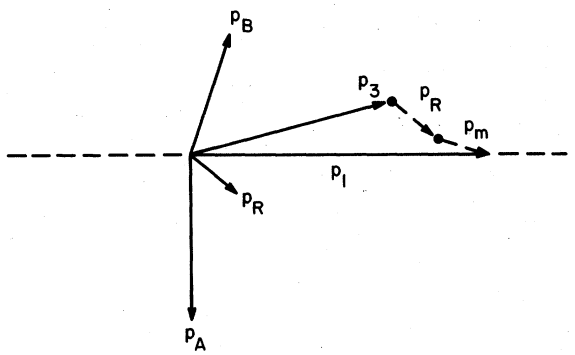

FIG. 2. Schematic diagram of momentum balance in the heavy ion reaction followed by fission of the target residue.

surement, whereas the momentum components perpendicular to the beam axis are only poorly known. This is primarily a result of placing the position sensitive detectors symmetrically about the beam axis, which gives $\langle\theta_A\rangle \simeq \langle\theta_B\rangle$. For an average event we can therefore write [see Eqs. (2) and (3)]

$$P_R^{\parallel} \simeq [(2M_A E_A)^{1/2} + (2M_B E_B)^{1/2}] \cos\theta_A \tag{8a}$$

and

$$P_R^{\perp} \simeq [(2M_A E_A)^{1/2} - (2M_B E_B)^{1/2}] \sin\theta_A . \tag{8b}$$

The primary energies E_A and E_B are closely related to the measured final energies, but the masses M_A and M_B are, in principle, unknown. An increase in the first term in Eq. (8a), due to the assumption of a large M_A, will be compensated by a decrease in the second term via M_B by mass conservation. Therefore, $P_R^{\parallel}$ is not very sensitive to the masses of the fission fragments. For the same reason, the perpendicular component of the recoil momentum, $P_R^{\perp}$, is very sensitive to the fragment masses M_A and M_B; see Eq. (8b).

For events that were detected in coincidence with a projectile residue (Li,...,O) we have made the following assumptions in order to be able to calculate the complete kinematics for each event:

$$M_R = M_2 \quad (\text{i.e., } M_m = M_1 - M_3) \tag{9}$$

and

$$P_R^{\perp} = -P_3^{\perp} \quad (\text{i.e., } P_m^{\perp} = 0) . \tag{10}$$

The first assumption introduces only minor uncertainties in the mass of the target residue prior to fission. The sensitivity to the second assumption was investigated in more detail by replacing it by the more general assumption of a constant value θ_m of the direction of the missing momentum vectors:

$$P_m^{\perp}/P_m^{\parallel} = \tan\theta_m = \text{const.} \tag{11}$$

The aim of this parametrization is to determine the range of the θ_m values, which will produce balanced mass distributions i.e., $\langle M_A\rangle \simeq \langle M_B\rangle$, a requirement which must be fulfilled for truly sequential fission decay. Assuming a constant value of θ_m, we can now solve the kinematics of the reaction. Defining

$$\overline{P}_4 = \overline{P}_1 - \overline{P}_3 \tag{12}$$

and using Eq. (7) we can rewrite Eq. (11):

$$P_R^{\perp} = P_R^{\parallel} \tan\theta_m + P_4(\sin\theta_4 - \cos\theta_4 \tan\theta_m) . \tag{13}$$

By inserting the expressions for $P_R^{\parallel}$ and $P_R^{\perp}$ from Eqs. (2) and (3) we find

$$P_B^2 C_B^2 = P_A^2 C_A^2 + P_4^2 C_4^2 - 2C_A C_4 P_A P_4 , \tag{14}$$

where

$$\begin{aligned} C_A &= \sin\theta_A - \cos\theta_A \tan\theta_m , \\ C_B &= \sin\theta_B + \cos\theta_B \tan\theta_m , \\ C_4 &= \sin\theta_4 - \cos\theta_4 \tan\theta_m . \end{aligned} \tag{15}$$

Rewriting Eqs. (4) and (5) gives

$$P_B = [(2M_R - P_A^2/E_A)E_B]^{1/2} , \tag{16}$$

and with Eq. (14),

$$\left(C_A^2 + C_B^2 \frac{E_B}{E_A}\right) P_A^2 - 2C_A C_4 P_4 P_A + C_4^2 P_4^2 - 2C_B^2 M_R E_B = 0 . \tag{17}$$

The solution to this equation is

$$P_A = \frac{C_A C_4 P_4 + C_B\left[2M_R E_B\left(C_A^2 + C_B^2 \frac{E_B}{E_A}\right) - C_4^2 P_4^2 \frac{E_B}{E_A}\right]^{1/2}}{C_A^2 + C_B^2 \frac{E_B}{E_A}} . \tag{18}$$

The remaining unknown quantities can then be obtained from the following relations,

$$M_A = P_A^2/2E_A , \tag{19a}$$

$$M_B = M_R - M_A , \tag{19b}$$

$$P_B = (2M_B E_B)^{1/2} , \tag{19c}$$

and from Eqs. (2), (3), and (7).

Mass dependent corrections for pulse height defects in the position sensitive detectors and for neutron evaporation from the fission fragments are performed by means of an iterative procedure for each event. The average number of neutrons emitted per fission is assumed to be

$$\overline{\nu}(M_R, E^*) = 0.118(M_R - 220) + 0.133E^* , \tag{20}$$

where E^* is the excitation energy of the fissioning system. This formula represents a reasonable average fit to experimental data.[18] The number of neutrons emitted from each fragment is, furthermore, assumed to be proportional to the fragment mass

$$\overline{\nu}(M_R, E^*, M_A) = \frac{M_A}{M_R}\overline{\nu}(M_R, E^*) . \tag{21}$$

The mass defect correction procedure was taken from Ref. 17. The dependence of the extracted mean values of $P_m^{\parallel}$ and $P_R^{\parallel}$ on the correction for neutron evaporation from the fragments is extremely insignificant. However, it should be kept in mind that the widths of the $P_R^{\parallel}$ distributions are artificially widened because neutron evaporation introduces random fluctuations on the angles θ_A and θ_B and on the final fragment energies and masses.

The momentum component $P_R^{\parallel}$ is rather insensitive to the choice of θ_m. This is illustrated in

Fig. 3 where the dependence of the average momentum components $\langle P_R^{\perp}\rangle$ and $\langle P_R^{\parallel}\rangle$, on θ_m is shown for the reaction ^{238}U(^{16}O, ^{10}Bf). Whereas $\langle P_R^{\perp}\rangle$ is rather sensitive to the particular choice of θ_m, there is only little dependence of $\langle P_R^{\parallel}\rangle$ on θ_m. Consequently, only the momentum components parallel to the beam axis are well determined. The range of acceptable choices of θ_m can be determined from the requirement that, on the average, both detectors should see equal amounts of light and heavy fission fragments, i.e., $\langle M_B - M_A\rangle = 0$. This requirement is a consequence of assuming that the fission decay occurs as a truly sequential process. This dependence of $\langle M_B - M_A\rangle$ on θ_m is shown in the upper part of Fig. 3. Within the accuracy of the present experiment, the range of acceptable values for θ_m falls between $-30°$ and $+5°$. Very similar observations are made for the other exit channels where a projectile residue was detected in coincidence with two fission fragments. In all cases the value $\theta_m = 0$ was found to lie within the range of acceptable values of θ_m, as deduced from the requirement $\langle M_B - M_A\rangle \simeq 0$.

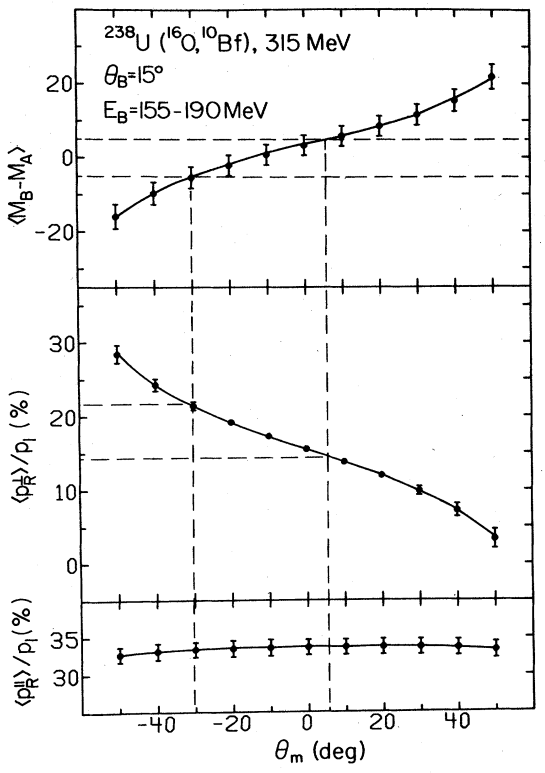

FIG. 3. The average mass difference $\langle M_B - M_A\rangle$ of fission fragments detected in the two fission counters; the average tranverse momentum of the recoiling nucleus $\langle P_R^{\perp}\rangle$ and the average longitudinal recoil momentum $\langle P_R^{\parallel}\rangle$ are shown as a function of the assumed angle of emission of the missing mass. Note the extreme insensitivity of $\langle P_R^{\parallel}\rangle$ on θ_m over the range of θ_m, where approximate balance of fission fragment masses in the two detectors is achieved.

We have, therefore, proceeded by using $\theta_m = 0$, i.e., Eq. (10), for the analysis of projectile residue—fission fragment coincidences. The uncertainties in the deduced momenta were estimated by varying the value of θ_m in the range between $-30°$ and $+30°$.

The value of $P_R^{\parallel}$ is mainly determined by the folding angle $\theta_{AB} = \theta_A + \theta_B$ between the two coincident fission fragments. This is illustrated in Fig. 4, which shows the distribution of the experimental data in a two dimensional θ_{AB} vs $P_R^{\parallel}$ contour plot. [For the calculation of the $P_R^{\parallel}$ values, assumptions corresponding to Eqs. (9) and (10) have been made.] For comparison, we have made a computer simulation of the fission decay of ^{238}U and ^{254}Fm and calculated the expected average folding angle[19] for our detector geometry by assuming that the momenta of these nuclei are parallel to the beam axis. The dependence of the expected average folding angles on the momentum of the fissioning nucleus is shown by the solid lines in Fig. 4 (and, similarly, in Fig. 5). The relatively small difference between the two lines illustrates the small uncertainty that is introduced by the assumption of Eq. (9). Note, that $M_R = 254$ is most unrealistic (i.e., impossible) for reactions where a coincident projectile residue is detected.

For central collisions that do not involve the production of a heavy projectile residue (Li, . . . , O)

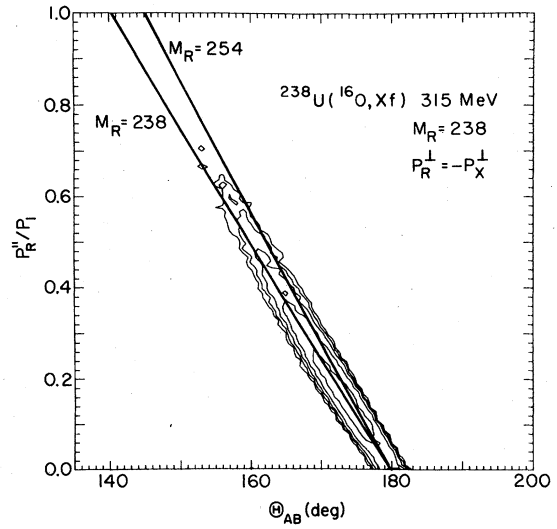

FIG. 4. Distribution of projectile residue—fission coincidence events in the $P_R^{\parallel}$ vs θ_{AB} plane. The assumptions of Eqs. (9) and (10) have been used for the analysis. The solid lines correspond to the calculated average quantities for the fission of ^{238}U and ^{254}Fm nuclei moving parallel to the beam axis.

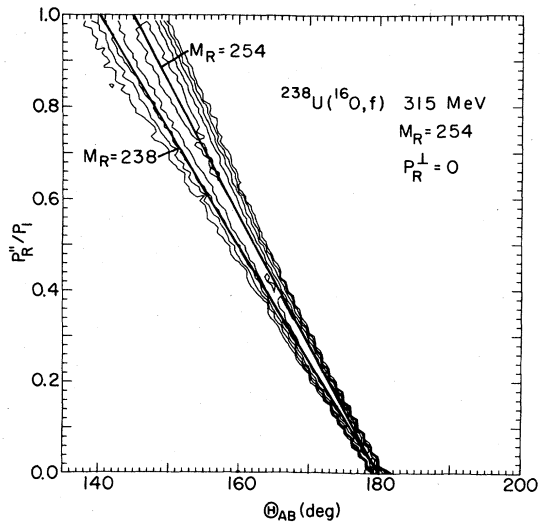

FIG. 5. Distribution of inclusive fission events in the $P_R^{\parallel}$ vs θ_{AB} plane. The assumptions of Eqs. (22b) and (22c) have been used for the analysis. The solid lines correspond to the calculated average quantities of ^{238}U and ^{254}Fm nuclei moving parallel to the beam axis.

in the exit channel the assumptions of Eqs. (9) and (10) are less realistic. In fact, if a compound nucleus is formed, one has the relations

$$P_R^{\parallel} = p_1 , \tag{22a}$$

$$P_R^{\perp} = 0 , \tag{22b}$$

$$M_R = M_1 + M_2 , \tag{22c}$$

and all kinematic qualities are (over) determined. For the analysis of inclusive fission events (where no coincident particle is required) and for the analysis of events involving only a coincident light particle ($p, \ldots, \alpha$), we have used a different set of assumptions for the analysis, requiring the validity of Eqs. (22b) and (22c). These assumptions are, obviously, good for reactions involving large transfers of linear momentum and mass. They are, however, poor for peripheral reactions. The distribution of inclusive fission events in the $P_R^{\parallel}$ vs θ_{AB} plane obtained with these assumptions is shown in Fig. 5. A comparison with Fig. 4 shows that the simple measurement of the folding angle already provides a good estimate about the mean value of the momentum transfer to the target residue. In this sense we can establish a relation between the value of θ_{AB} and $P_R^{\parallel}$. This has been done in Fig. 9 of the following section by using the solid curve corresponding to fission of ^{254}Fm.

IV. RESULTS

The experimental results naturally divide into two subgroups, namely, (1) energy spectra of emitted particles and folding angle distributions, and (2) distributions of missing momentum, fission fragment mass, energy, etc., which result from an event by event reconstruction of the kinematics of the reaction. The latter group of data is thus somewhat dependent on the assumptions made in the reconstruction.

A. Projectile residue energy spectra

Energy spectra of heavy ions observed in the triple telescope at 15° in coincidence with fission fragments are shown in Fig. 6. These spectra were recorded close to the grazing angle of $\theta_g \approx 19°$ and exhibit close similarities to inclusive spectra of projectile residues[20] observed at 15° in ^{16}O induced reactions on ^{208}Pb at 315 MeV. From this qualitative similarity we conclude that the requirement of a fission coincidence does not impose a serious kinematical bias on the spectra. Such a bias is only present in the ^{16}O spectrum which, of course, exhibits a sharp cutoff that corresponds to the fission threshold of ^{238}U.

The energy spectra shown in Fig. 6 have maxima that correspond to the velocities of the projectile residue close to the beam velocity (marked by arrows). The widths of the energy spectra increase with decreasing atomic numbers of the outgoing projectile residues. These observations are similar to the ones for inclusive spectra,[20] which could be explained within the framework of a simple model for projectile fragmentation.[21,22] It has been shown[21,22] that the widths of these energy spectra can either be explained in terms of the Fermi momenta of the nucleons in the projectile if a fast breakup process is assumed, or they can be explained in terms of the thermal kinetic energy of the nucleons in the projectile if the reaction proceeds via the sequential decay of an excited and completely thermalized projectile.

At present, several partly conflicting models[23-25] have been proposed to understand the characteristics of such inclusive energy spectra, ranging from simple transfer reactions to breakup processes. From these investigations it has become apparent that more detailed experimental investigations are required to limit the number of possible interpretations.

B. Light particle energy spectra

Laboratory energy spectra for light charged particles (p, d, t, and α) detected at $\theta_{lab} = 14°$ in coincidence with fission fragments are shown in Fig. 7. At this angle, the maximum cross section is observed for the emission of alpha particles. However, very sizable intensities are also observed for the emission of protons, deuterons,

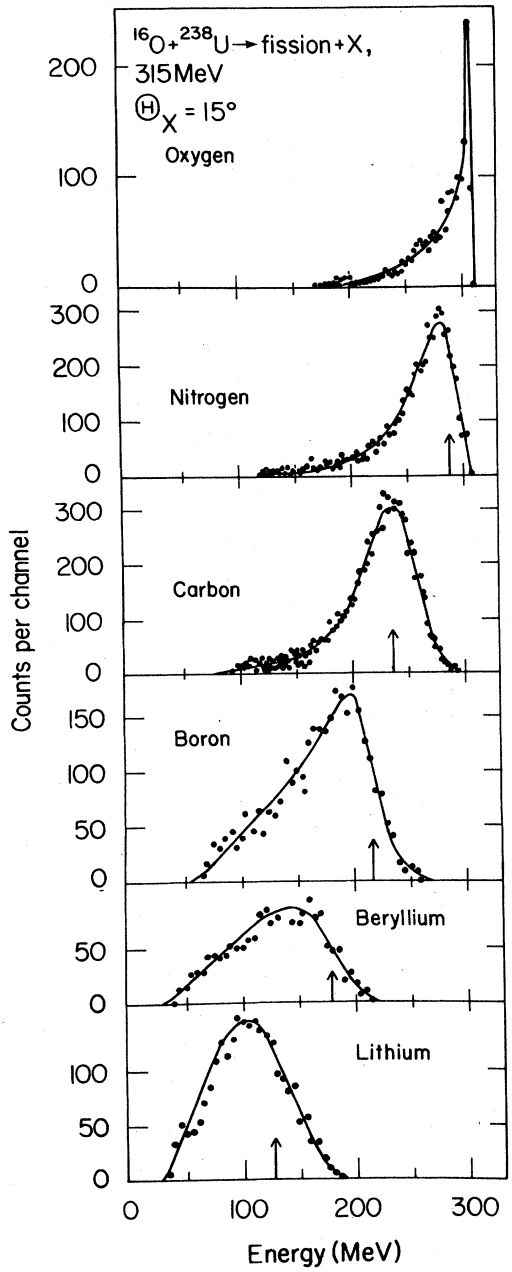

FIG. 6. Laboratory energy spectra of projectile fragments (Li–O) detected in the heavy ion telescope at $\theta = 15°$, in coincidence with fission fragments.

and tritions. The cross sections for the emission of p, d, and t differ by no more than a factor of 2. (Note that the emission of deuterons and tritons is generally considered to be of minor importance[26] for compound nucleus evaporation.) The spectra are characterized by fairly flat slopes at the high energy side of the spectrum, which extends far above the energy corresponding to the beam velocity. It should be clear that these flat slopes

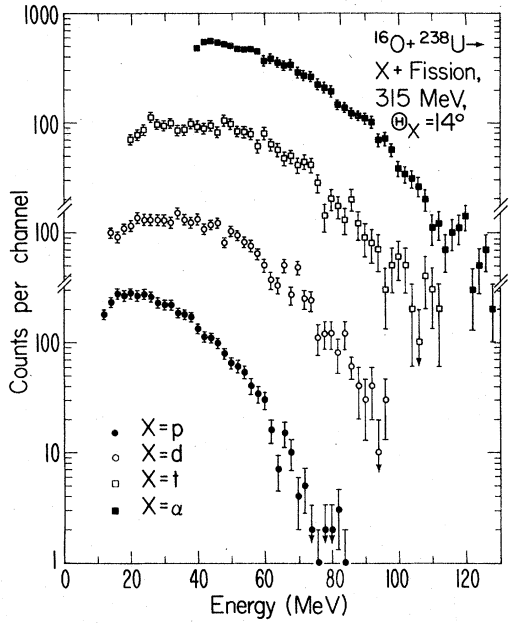

FIG. 7. Laboratory energy spectra of light ions (p, d, t, and α) detected in the Si-NaI telescope positioned at $\theta = 14°$ in coincidence with the fission fragments.

cannot be understood in terms of evaporation from the compound nucleus.[11,16] This is particularly clear for the proton spectrum, which has a tail up to four times the energy corresponding to the beam velocity. This energy interval corresponds to the range of energies expected for "promptly emitted particles,"[27] which could possibly give a strong contribution to the proton spectrum at forward angles. The theory for promptly emitted particles relies on a vector addition of the Fermi velocity of nucleons in the projectile and relative velocity of projectile and target, and has not yet been extended to the emission of complex particles. The large cross sections that are observed for protons, as well as for deuterons and tritons, clearly require a theory that treats the emission of complex particles on a footing similar to the emission of nucleons.

A comparison of α-particle spectra from all three light particle telescopes is presented in Fig. 8. All three spectra exhibit rather similar qualitative features, indicating that the emission of energetic alpha particles is not restricted to the entrance channel grazing angle or to the plane of the two fission fragments.

C. Fission fragment folding angle distributions

Several aspects of the reaction mechanism are directly observable by studying the folding angle distribution of fission fragments as illustrated in Fig. 9. The folding angle θ_{AB}, indicated by the

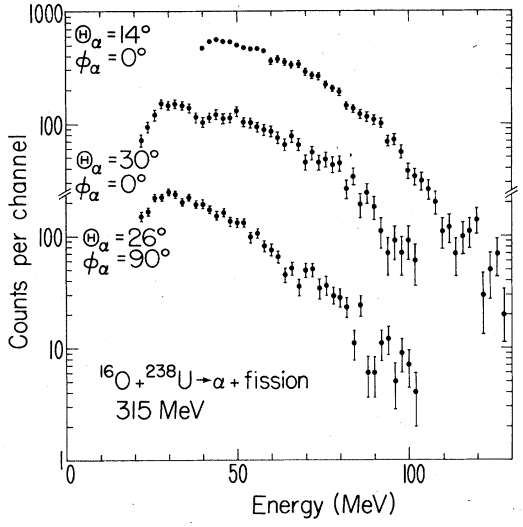

FIG. 8. Laboratory energy spectra of α particles detected in coincidence with fission fragments with the Si-NaI telescope (upper set of data points), the 30° in plane α telescope, and the 26° out of plane α telescope (lower set of data points).

scale at the bottom of the figure, is defined as the angle of emission between the two fission fragments measured in the laboratory system. The scale for linear momentum transfer, shown at the top of the figure, has been calculated assuming fission of ^{254}Fm, which is the compound nucleus resulting from fusion of ^{16}O and ^{238}U. This calibration corresponds to the solid lines marked by ^{254}Fm in Figs. 4 and 5. The mean folding angle expected for fission of the compound nucleus ($P_R = P_1$) is $\theta_{AB} = 144.4°$ and is marked by a vertical dashed line in the figure. The folding angle distribution for inclusive fission events exhibits two clearly separated components. The strongest component is centered at $\theta_{AB} = 148°$ corresponding to ~92% of the beam momentum being transferred to the fissioning system. We associate this group with "central" collisions that involve a large overlap between target and projectile and are dominated by fusion, "incomplete" fusion,[28] or "massive transfer"[29] reactions.

The second component in the folding angle distribution, which peaks at $\theta_{AB} \simeq 173°$, can be attributed to "peripheral" reactions in which the major part of the projectile momentum is carried off by heavy projectile residues exhibiting angular distributions with strong forward peaking.[20] The minimum in the folding angle distribution reflects the fact that, for peripheral reactions, the largest cross sections are observed for nitrogen and carbon fragments and larger mass transfers are less likely.

The distributions of fission fragment folding angles measured in coincidence with light charged particles (p, d, t, and α) detected at $\theta = 14°$ are also shown in the figure. The folding angle distribution gated on protons still exhibits two maxima indicating that the protons originate not only from

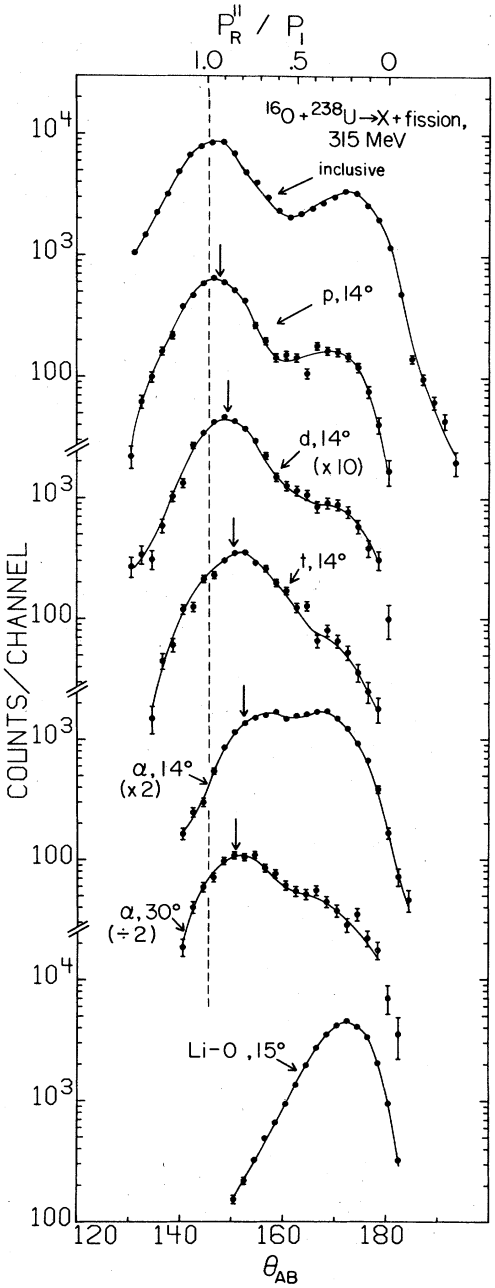

FIG. 9. Folding angle distributions of fission fragments measured inclusively (top), in coincidence with protons, deuterons, tritons, and α particles in the $\theta = 14°$ Si-NaI telescope, in coincidence with α particles in the $\theta = 30°$ in-plane telescope, and in coincidence with heavy projectile residues (Li–O) in the heavy ion telescope at $\theta = 15°$.

massive transfer or incomplete fusion reactions leading to large recoil momenta, but also from peripheral reactions, where the major part of the beam momentum is carried off by projectile-like fragments. This small momentum transfer group decreases in intensity when observed in coincidence with deuterons and tritons. The maxima in the distributions shift to larger folding angles when going from fission inclusive to triton coincident events. This effect is a consequence of linear momentum conservation, since part of the beam momentum is carried off by the detected light particle. The arrows in the figure indicate the position at which the recoil momentum is equal to the difference between the beam momentum and the mean momentum carried by the coincident light particle. The fact that these arrows coincide rather closely with the maxima for p, d, and t coincidences indicates that the multiplicity of fast light particles emitted in the forward direction is not significantly larger than that for incomplete fusion events. This observation does not apply to α-particle coincidences, which show a rather broad folding angle distribution indicating very large contributions from peripheral reactions or a multiplicity of fast forward directed α particles of more than two. This is not too surprising, since fast forward directed α particles are expected to result from several different reactions ranging from massive transfer of ^{12}C to α-particle breakup of the ^{16}O projectile. The situation is somewhat different when α particles are detected at 30°. Here the relative importance of projectile breakup processes is smaller, and a peak at smaller folding angles appears.

It is interesting to use the folding angle of the fission fragments to classify "peripheral" and "central" collisions and to study the corresponding spectra of coincident light particles. We have, therefore, introduced a cut at $\theta_{AB}=160°$ and defined events with smaller folding angles ($\theta_{AB}<160°$) as central collisions and events with larger folding angles ($\theta_{AB}>160°$) as peripheral collisions. Energy spectra of light particles (p, d, t, and α) emitted at $\theta_{NaI}=14°$ are shown in Fig. 10 for both central and peripheral events. Although there are differences in the low energy regions of these spectra, it is most remarkable that very similar slopes are observed in the high energy region of the spectra. Within the present statistics these slopes can be rather well described by an exponential shape $\exp(-E/T)$ with $T=13$ MeV, and little systematic variation is detected for the emission of p, d, t, and α particles between central and peripheral collisions. This observation was verified to be independent of the particular choice of division between central and peripheral reactions. This

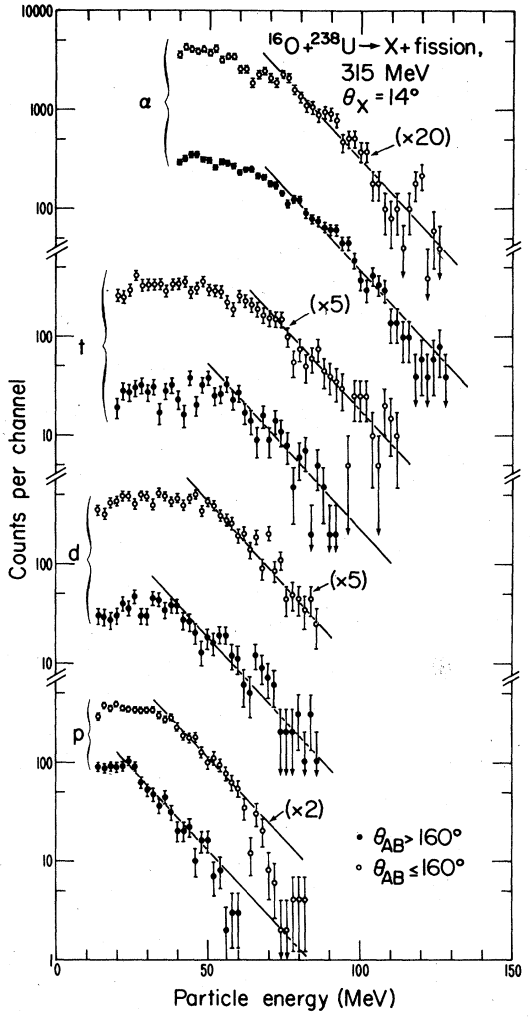

FIG. 10. Laboratory energy spectra of protons, deuterons, tritons, and α particles detected in the $\theta=14°$ Si-NaI telescope in coincidence with fission fragments with folding angles $\theta_{AB}<160°$ (open circles, central collisions) and with folding angles $\theta_{AB}>160°$ (filled circles, peripheral collisions).

similarity in the spectra strongly suggests that light particles observed in both central and peripheral collisions are of similar origin. This is most naturally explained by postulating that the light particles originate from the early stages of the collision, e.g., from projectile breakup mechanism, when the ultimate fate of the projectile residue is not yet determined. Thus the projectile residue could either fuse with the target nucleus or interact only relatively weakly by inelastic scattering or few nucleon transfer and emerge at small angles carrying off a large part of the beam momentum.

Despite the similarities, there are, however, some differences, especially between the proton

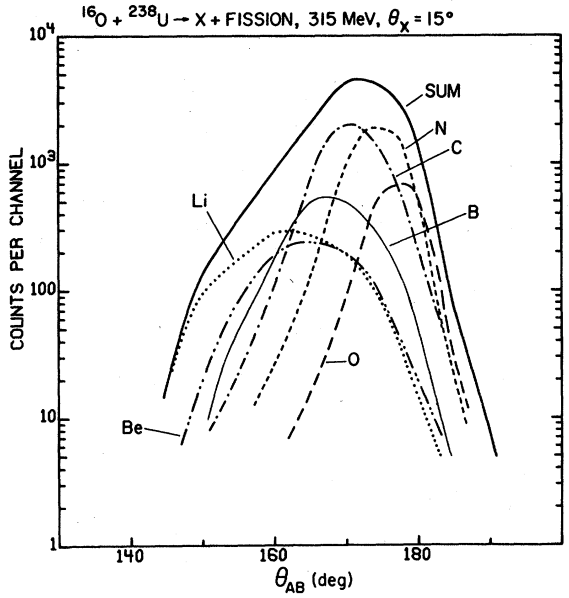

FIG. 11. Folding angle distributions of fission fragments measured in coincidence with projectile residues (Li, Be, B, C, N, and O) in the $\theta = 15°$ heavy ion telescope. The sum over all products from Li to O is shown as a solid line.

spectra for central and peripheral collisions. The low energy part of the spectrum for central collisions exhibits a flat region up to $E_p \simeq 32$ MeV, whereas this region extends only to $E_p \simeq 24$ MeV for peripheral collisions. The reason for this difference is not understood at present.

Folding angle distributions measured in coincidence with projectile residues (Li, Be, B, C, N, and O) at 15° are shown in Fig. 11. As expected from momentum conservation requirements these folding angle distributions peak at angles closer to the zero momentum transfer limit ($\theta_{AB} = 180°$), with increasing mass of the outgoing projectile residue. (Remember, that the velocity of the projectile residues is close to the beam velocity.) However, the more detailed analysis of the data described in the following subsection shows that the momentum carried off by the projectile-like fragment cannot account for the difference between the beam momentum and the recoil momentum of the fissioning system.

D. Missing momentum distributions

A more detailed description of the reaction mechanism can be obtained by performing an event by event reconstruction of the kinematics of the reaction as described in Sec. III. This type of analysis has been applied to that part of the data which involved detection of a projectile-like fragment (Li, . . . , O) at $\theta = 15°$ in coincidence with both fission fragments. The purpose of applying this type of analysis is to obtain missing momentum distributions and fission fragment mass distributions.

Missing momentum distributions are shown in Figs. 12–15 for various projectile residues and cuts in the energy spectra. The missing momentum distribution for the highest energy cut on inelastically scattered ^{16}O ions is centered around zero, since only pure inelastic scattering (followed by fission) is energetically possible. This provides a stringent test of the absolute calibration of the folding angles. However, the missing momentum distributions for the two lowest energies of the scattered ^{16}O ions show a clear shift away from zero missing momentum. Similar trends are observed for lighter projectile fragments as illustrated in Figs. 13–15. Arrows in the figures represent the missing momentum expected for quasielastic projectile breakup reactions, where the projectile breaks up into two or more fragments and where the undetected particles continue with the beam velocity. The missing momentum distributions are peaked between the pure two-body reaction limit $\langle P_m \rangle = 0$ and the quasielastic projectile breakup limit $\langle P_m^{\parallel} \rangle = [(M_1 - M_3)/M_1]P_1$. The rather narrow widths of the $P_m^{\parallel}$ distribution indicate that the main reaction mechanism is not a simple superposition of simple transfer reactions and quasielastic breakup reactions.

The systematics of the average missing momentum as a function of the energy of the projectile residue is shown in Fig. 16. The data points are scattered around a line with a negative slope of $\langle P_m^{\parallel} \rangle / P_1 \langle E_3 \rangle = 1.0 \times 10^{-3}$ MeV^{-1}. The missing

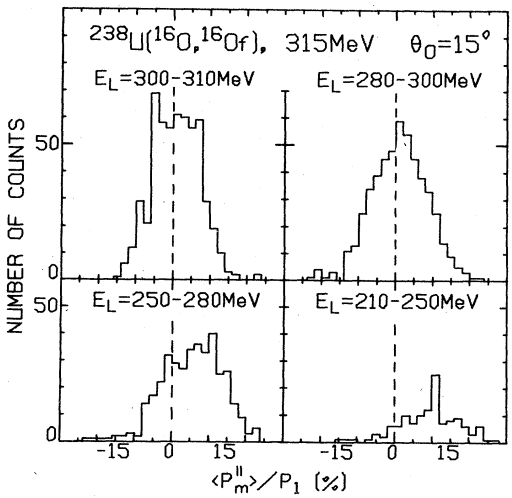

FIG. 12. Missing momentum distributions for four different gates on the laboratory energy of outgoing ^{16}O ions. $\langle P_m^{\parallel} \rangle$ is positive in the beam direction.

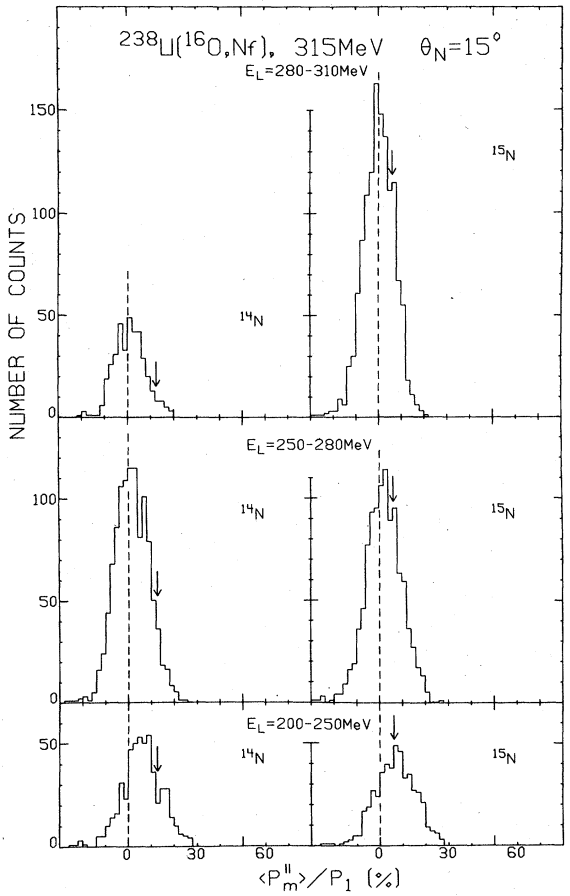

FIG. 13. Missing momentum distributions for three different gates on the laboratory energy of ^{14}N and ^{15}N projectile residues. $\langle P_m^{\parallel}\rangle$ is positive in the beam direction.

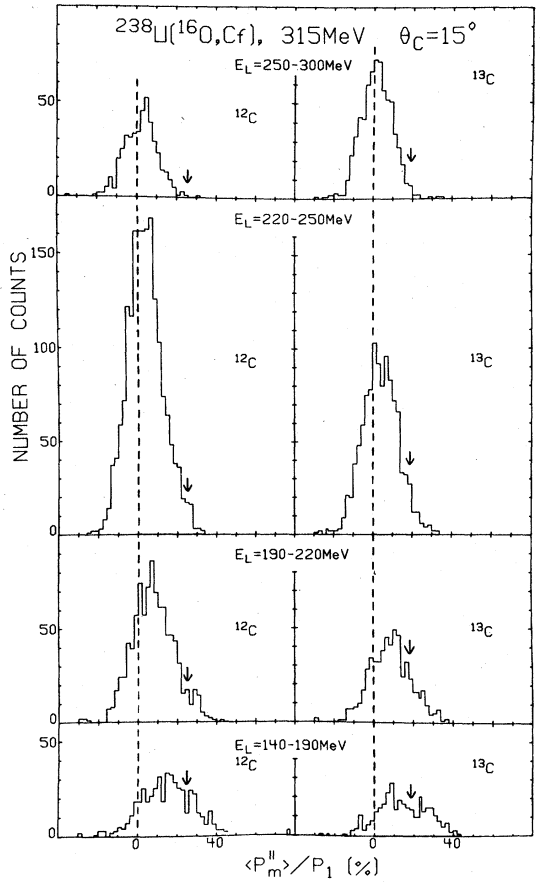

FIG. 14. Missing momentum distributions for four different gates on the laboratory energy of ^{12}C and ^{13}C projectile residues. $\langle P_m^{\parallel}\rangle$ is positive in the beam direction.

momentum increases with increasing energy loss of the projectile residue. Such a behavior is consistent with any mechanism that associates the energy loss with the emission of light particles into the forward direction. In particular, the sequential decay of the projectile residue by light particle emission would be consistent with the trends observed in Fig. 16 since larger energy losses would be associated with higher excitation energies of the projectile residue and this, in fact, would lead to a higher multiplicity of light particles emitted from the projectile residue. However, this picture would require a different reaction mechanism for the production of energetic light particles in peripheral collisions as compared to central collisions where no projectile residue is observed in the exit channel. Although this possibility cannot be ruled out in a rigorous way, we feel that such an interpretation is not likely because of the similarity of the light particle spectra in central and peripheral collisions (see the discussion of Figs. 9 and 10), which suggested that the majority of the light particles observed at forward angles is produced at an early stage of the reaction.

The dependence of the average value of the recoil momentum $\langle P_R^{\parallel}\rangle$ on the average momentum of the projectile residue $\langle P_3^{\parallel}\rangle$ is shown in Fig. 17. For a pure two-body reaction (followed by fission of the target residue) one has $P_1 = P_R^{\parallel} + P_3^{\parallel}$. For orientation, this limit is shown by the solid line in the figure. The data clearly rule out this limit, as was already obvious from Figs. 12–15. The extreme limit of quasielastic projectile breakup, where the target nucleus acts as a mere spectator, corresponds to negligibly small values of $P_R^{\parallel}$ similar to the ones observed for inelastic scattering. This process was consistent with the single particle inclusive spectra,[21] however, it was not consistent with the rather large values of $P_R^{\parallel}$ observed in the present experiment. The reaction, instead,

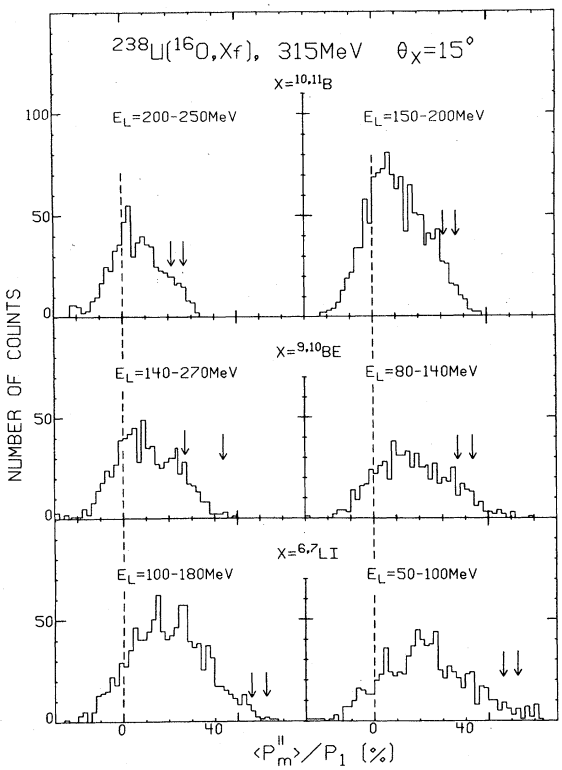

FIG. 15. Missing momentum distributions for two different gates on the laboratory energy of ^{10,11}B, ^{9,10}Be, and ^{6,7}Li projectile residues. $\langle P_m'' \rangle$ is positive in the beam direction.

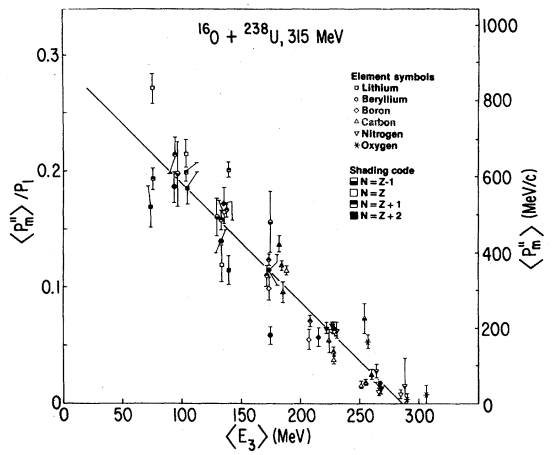

FIG. 16. Dependence of the average missing momentum on the laboratory energy of the projectile residue.

involves significant interaction between projectile and target. Note that the extreme participant spectator model[30] was originally developed to explain inclusive spectra observed in heavy ion induced reactions at high energy and has not yet been subject to the more crucial test of coincidence experiments.

E. Fission fragment mass distributions

As discussed in Sec. IV C, the measurement of the fission fragment folding angles provides im-

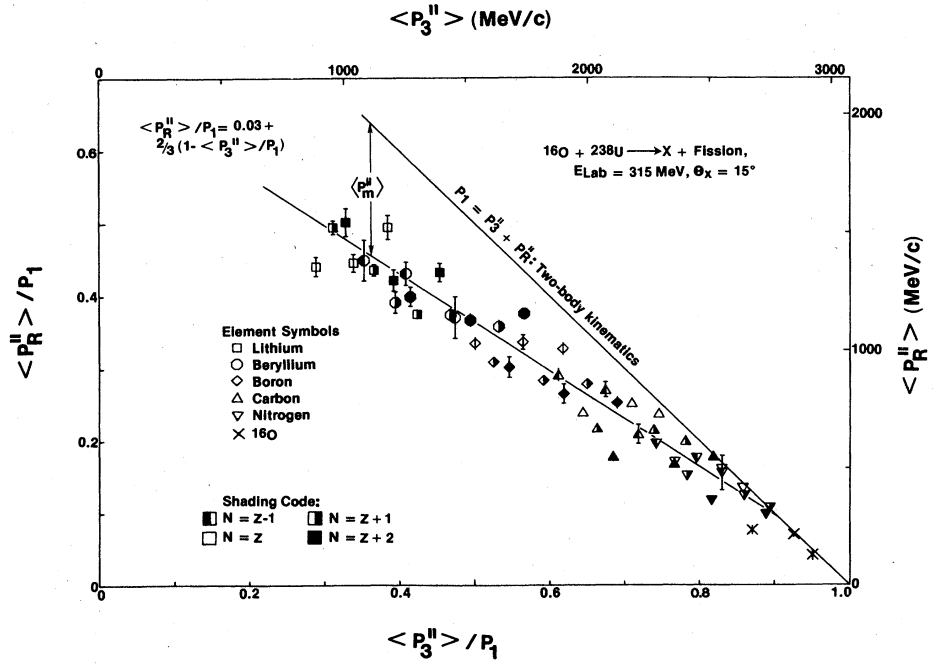

FIG. 17. Dependence of the average parallel component of the recoil momentum on the average parallel component of the momentum of the projectile residue. The limit expected for pure two-body reactions is indicated and the average missing momentum can be derived as the distance from this line to the data points.

portant information about the momentum transfer to the recoil nucleus. Similarly, we can obtain an estimate of the excitation energy of the fissioning system from the mass distribution of fission fragments. The mass distributions measured in coincidence with the projectile residues Li,...,O are shown in Figs. 18–21 for several regions of the outgoing particle energies. For the high kinetic energy region of the oxygen and nitrogen spectra we observe very asymmetric mass distributions with large (>20) peak-to-valley ratios. Such asymmetric mass distributions are typical for the fission of actinide nuclei at relatively low excitation energies. The valley corresponding to symmetric fission (the mass of the fissioning nucleus was assumed to be $M_R = 238$ in this analysis) is seen to fill in for increasing energy losses. This indicates that fission takes place from a more highly excited nucleus. For asymmetric fission fragment mass distributions, one can put this qualitative observation on a more quantitative basis by comparing the peak to valley ratios of these mass distributions with the ones observed in reactions where the excitation of the fissioning nucleus is known, and thus obtain an estimate of the excitation energy for each ejectile energy bin. The results of such a comparison with mass distributions obtained in measurements of fission following compound nucleus formation in the α bombardment of a ^{238}U target[31] (see Fig. 22) are presented in Table I.

For the smallest energy losses, as observed for high energy oxygen and nitrogen nuclei, the target residue excitation energy, which is deduced from the fission fragment mass distributions, is slightly larger than allowed even for a two-body reaction. The reason for this is the relatively poor energy resolution of the position sensitive fission detectors, which fills in the valley between the two mass peaks. However, for larger energy losses of the outgoing projectile residues the fission fragment mass distributions observed experimentally are more asymmetric than expected from an estimate of the excitation energy on the basis of two-body kinematics. In fact, the assumption of two-body kinematics can lead to a significant overestimate of the target residue excitation energy. On the other hand, it is also clear that the amount of excitation energy deposited in the target residue is by no means negligible. This corroborates the conclusion drawn from the large momentum transfers to the target residue that inelastic interactions with the target are an important aspect of the reaction mechanism. Quasielastic breakup is not the dominant reaction mechanism. Similar conclusions had been drawn[32] from

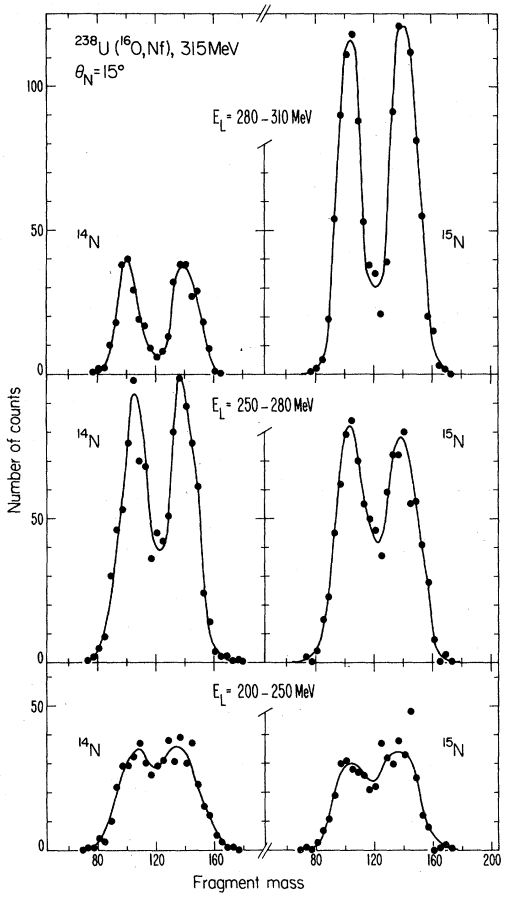

FIG. 19. Mass distributions of fission fragments for three different gates on the ^{14}N and ^{15}N laboratory energy.

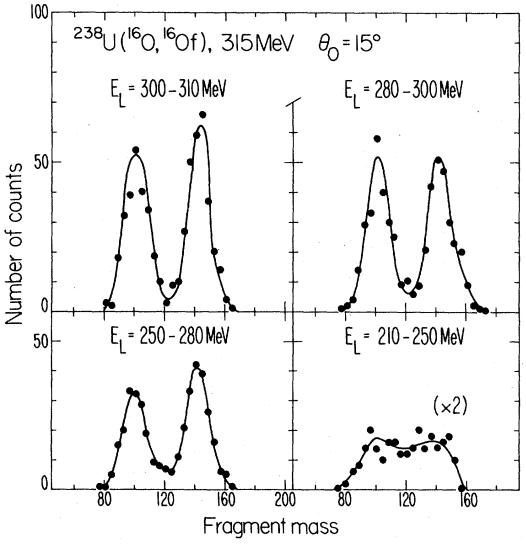

FIG. 18. Mass distributions of fission fragments for four different gates on the ^{16}O laboratory energy.

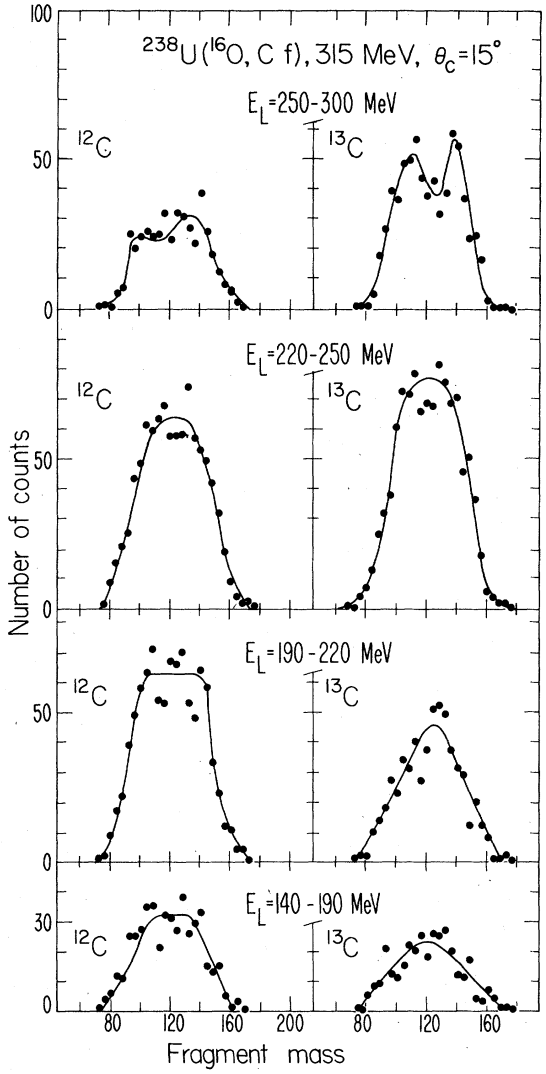

FIG. 20. Mass distributions of fission fragments for four different gates on the ^{12}C and ^{13}C laboratory energy.

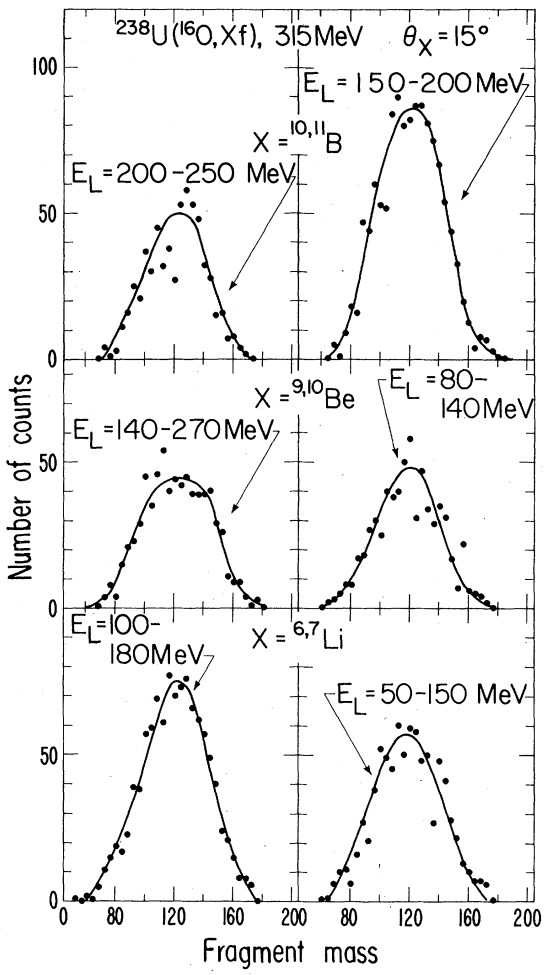

FIG. 21. Mass distributions of fission fragments for two different gates on the laboratory energy of ^{10,11}B, ^{9,10}Be, and ^{6,7}Li projectile residues.

the measurement of alpha-particle projectile-residue coincidences. The analysis of that experiment, however, had to rely on the validity of three body kinematics in order to deduce the excitation energy of the target residue.

V. SUMMARY AND CONCLUSION

In the present experiment we have studied the fission decay of the target residue in coincidence with projectile residues or light particles produced in ^{16}O-induced reactions on ^{238}U at 20 MeV/nucleon beam energy. The measurement of the folding angle between coincident fission fragments was shown to provide valuable information on the linear momentum transferred to the target residue prior to fission.

A detailed analysis of missing momentum and fission fragment mass distributions, observed in coincidence with projectile residues at 15°, has provided clear evidence for the inadequacy of the assumption of two-body kinematics for obtaining information on the excitation energy of the target residue. The emission of light particles into the forward direction is an important aspect of the reaction mechanism. However, the emission of light particles is not due to a quasielastic breakup process where the target nucleus acts as a mere spectator. Instead, large amounts of linear momentum and excitation energy are transferred to the target nucleus during the collision. Future extensions of models for heavy ion breakup reactions will have to include this large inelasticity of the reaction. Such information could not be obtained from the study of single particle inclusive

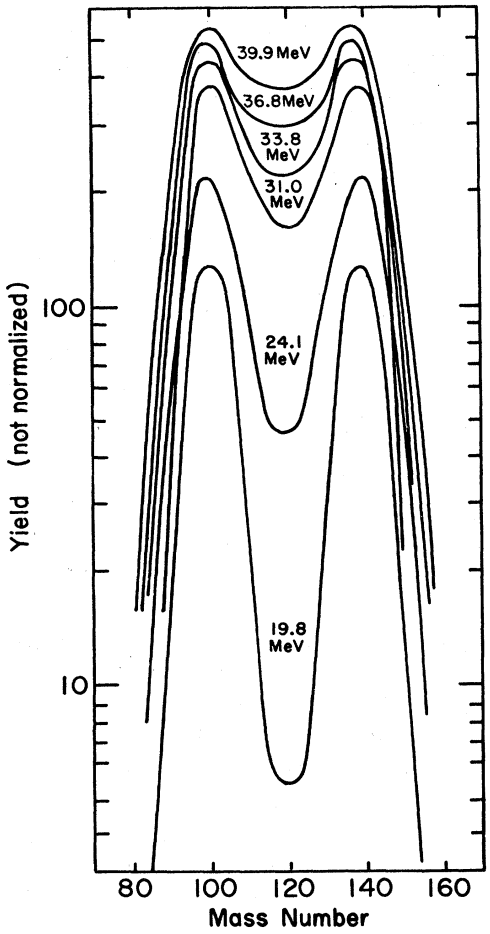

FIG. 22. Fission fragment mass distributions for α induced fission of ^{238}U at projectile energies indicated in the figure. The data are taken from Ref. 31.

energy spectra, which could be rather well described by quasielastic projectile breakup processes.[21-24] It will be interesting to extend similar studies to higher projectile energies where the simple participant-spectator models have been applied most successfully to describe single particle inclusive cross sections.

When measured in coincidence with light particles, the folding angle between two fission fragments can be used for a simple overall classification of the reaction into peripheral (i.e., low momentum transfer) and central (i.e., large momentum transfer) reactions. The majority of high energy protons emitted at 14° was shown to be associated with central collisions. It was shown that the multiplicity of energetic light particles emitted into the forward direction was no larger than about 1. This rules out a fireball mechanism, which has been rather successful in the description of single particle inclusive proton spectra. The

TABLE I. Estimates of excitation energy of the fissioning nucleus.

Ejectile	E_3 (MeV)	$\langle E^*(E_3)\rangle$[a] (MeV)	$\langle E^*(P/V)\rangle$[b] (MeV)
^{16}O	300–310	7.4	<14
	280–300	22.2	16
	250–280	46.6	18
	210–250	78.7	35
^{15}N	280–310	16.5	20
	250–280	39.0	28
	200–250	75.3	33
^{14}N	280–310	14.0	17
	250–280	34.3	25
	200–250	67.7	35
^{13}C	250–300	38.7	33

[a] Average excitation energy of the fissioning system estimated from the ejectile energy assuming two-body kinematics.

[b] Average excitation energy of the fissioning system estimated from the peak/valley ratio of the mass distribution when compared to $\alpha + ^{238}U$ data of Ref. 31.

study of energetic light particles emitted at small angles ($\theta_{lab}=14°$) has revealed a striking similarity of the energy spectra observed in coincidence with central and peripheral collisions. This suggests a reaction mechanism in which the light particles are produced at an early stage of the reaction. An attractive possibility is the concept of a breakup reaction that can then be accompanied by inelastic scattering, a transfer reaction, or absorption between the target residue and one of the projectile fragments.

ACKNOWLEDGMENTS

We appreciate the effort and enthusiasm shown by the 88″-cyclotron operating staff in providing the difficult 315 MeV $^{16}O^{6+}$ beams for the present experiment. The help in solving mechanical and electronic problems extended to us by H. Wieman, M. Zisman, and W. Meyer is gratefully acknowledged. Excellent uranium and gold targets fabricated by Claude Ellsworth were essential for the successful completion of this study. This work is supported in part by the National Science Foundation under Grant No. Phy 7822696 and in part by the Office of Basic Energy Sciences, Division of Nuclear Sciences, U. S. Department of Energy.

APPENDIX: CORRECTION FOR SYSTEMATIC FOLDING ANGLE ERRORS

The small size (8 × 47 mm) of commercially available (ORTEC) position sensitive solid state detectors demands a close geometry of the ex-

perimental setup in order to facilitate a complete coverage of the folding angle distributions. This, in turn, renders the experimental determination of the folding angles very susceptible to systematic errors, which can arise from the beam not intercepting the target foil exactly at the center of the scattering chamber, with respect to which the angular calibration of the PSD's were performed. In order to minimize such uncertainties, we have performed a separate measurement of the fission inclusive folding angle distribution of ^{16}O incident onto ^{238}U at beam energies 315 and 140 MeV. Two main contributions to the systematic folding angle error arise from the fact that (1) the target plane might by slightly offset from the center of the chamber by an amount d, and (2) the beam misses the true center of the chamber by an amount y. A possible geometry is shown in Fig. 23. The center of the chamber is denoted C and the intercepts between the "ideal" and the "actual" beam axis with the target are denoted D and I, respectively. The two sides ID and CD in the triangle ICD are given by

$$ID = \frac{y}{|\sin\theta_t|}, \text{ and } CD = \frac{d}{|\sin\theta_t|}, \tag{A1}$$

the third side CI is given by

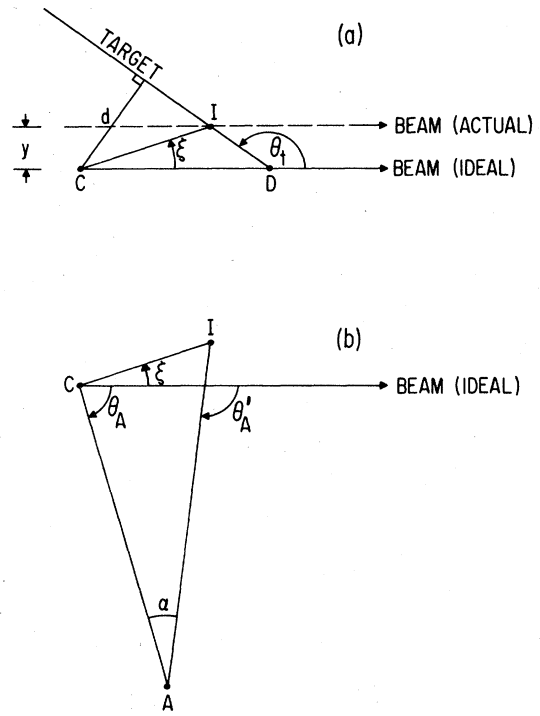

FIG. 23. Illustration of the effects of beam spot offsets. Trigonometric relations used to derive the angle corrections are discussed in the text.

$$CI = [CD^2 + ID^2 - 2\cdot CD\cdot ID\cdot\cos(\pi - \theta_t)]^{1/2}. \tag{A2}$$

The angle ξ between the beam axis and CI is

$$\xi = \arcsin(y/CI), \tag{A3}$$

where the solution in the interval $[0, \pi/2]$ is applicable if $CD/ID > \cos\theta_t$ and the solution between $\pi/2$ and π applies if $CD/ID < \cos\theta_t$ [see Fig. 23(a)].

The correction term α to the measured fission fragment angle θ_A can be derived from trigonometric relations, which applies to the triangle ACI shown in Fig. 23(b). Here the point A denotes the position where the fragment is detected in the PSD. Trigonometric relations give after reduction

$$\begin{aligned}\sin\alpha &= CI\cdot\sin(\alpha + \theta_A + \xi)/CA \\ &= CI\cdot[\sin\alpha\cos(\theta_A + \xi) + \cos\alpha\sin(\theta_A + \xi)]/CA.\end{aligned} \tag{A4}$$

After rearranging and squaring we obtain

$$\sin^2\alpha = \frac{CI^2\cdot\sin^2(\theta_A + \xi)}{CA^2 + CI^2 - 2\cdot CA\cdot CI\cdot\cos(\theta_A + \xi)} \tag{A5}$$

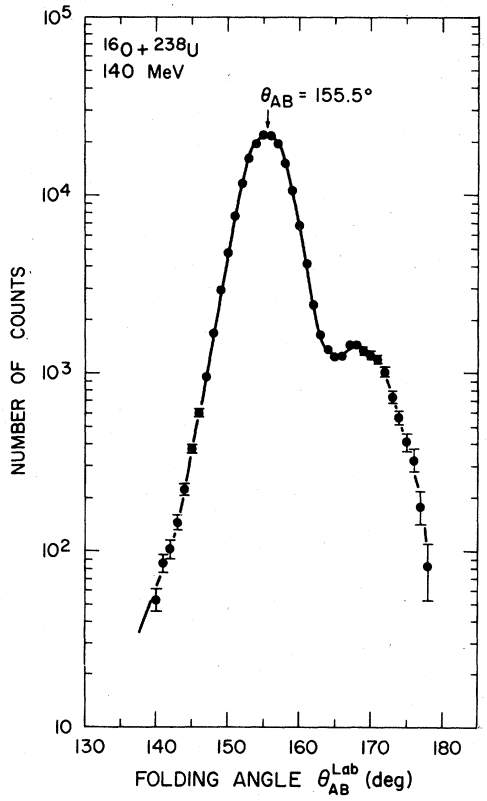

FIG. 24. Inclusive fission fragment folding angle distribution for 140 MeV ^{16}O on ^{238}U. Data have been corrected for systematic errors due to imperfect beam and target positions, as well as the folding angle dependent detection efficiency.

and finally

$$\alpha = \arcsin\left(\frac{CI\sin(\theta_A+\xi)}{[CA^2+CI^2-2\cdot CA\cdot CI\cdot\cos(\theta_A+\xi)]^{1/2}}\right). \quad \text{(A6)}$$

The solution in the interval $[-\pi/2,\pi/2]$ should be used. The true emission angle of the registered fission fragment is

$$\theta'_A=\theta_A+\alpha. \quad \text{(A7)}$$

The correction β which applies to fission fragments registered in PSD-*B* can similarly be written as

$$\beta = \arcsin\frac{CI\sin(\theta_B-\xi)}{[CB^2+CI^2-2\cdot CB\cdot CI\cdot\cos(\theta_B-\xi)]^{1/2}}, \quad \text{(A8)}$$

where *CB* is defined in analogy to *CA*. Again only the solution in the interval $[-\pi/2,\pi/2]$ should be used to compute the true emission angle θ_B, which is given as

$$\theta'_B=\theta_B+\beta. \quad \text{(A9)}$$

By measuring the inclusive folding angle distributions for four angles of the target with respect to the beam axis, namely θ, $\pi-\theta$, $\pi+\theta$, and $2\pi-\theta$, we can determine the two contributions to the systematic error rather accurately by requiring the corrected folding angle distributions to remain independent of target angle. Shifts in the inclusive folding angle distributions measured for three settings of the target angle are in fact sufficient for a determination of the two offsets and the true folding angle distribution, and consequently the fourth target angle setting serves as a consistency check of the measurement. The inclusive fission folding angle distribution resulting from 140 MeV ^{16}O incident on ^{238}U is shown in Fig. 24. These data, which are the sum of four target settings, have been corrected for systematic errors due to target and beam offsets. The maximum in the distribution is located at $\theta_{AB}=155.5°$, which is in excellent agreement with the theoretical estimate of $\theta_{AB}^{\text{theo}}=155.8°$ derived from the measured total kinetic energy (TKE) release[19] of 195.1 MeV for ^{254}Fm and the assumption of full momentum transfer to the compound nucleus. The same system (140 MeV ^{16}O + ^{238}U) has already been studied by Sikkeland *et al.*,[14] who restricted the detection of one fragment to $\theta_A=90°$ and measured the fission yield in the other detector. The maximum in the yield curve was located at $\theta_B=66.6°$, which corresponds to a folding angle of $\theta_{AB}=156.5°$. However, the discrepancy between this result and our measurement is a consequence of confining one detector to 90°. This is evident from a calculation of the expected most probable folding angle from the known total kinetic energy release under these kinematical circumstances. Such a calculation predicts $\theta_{AB}^{\text{theo}}=156.5$, which is identical to the experimental value. The ~1° discrepancy between the present experiment and the results of Ref. 14 can therefore be attributed to the slightly different experimental arrangements used in the two cases. We therefore conclude that the measurement of the folding angles in the present experiment is accurate to within ±1°. Measurements of the fission inclusive folding angle distribution were also performed at 315 MeV and the maximum in the distribution was located at $\theta_{AB}=148°$.

---

*Present address: Chemistry Division, University of Maryland, College Park, Maryland 20742.

[1]A. G. Artukh, G. F. Gridnev, V. L. Mikheev, V. V. Volkov, and J. Wilczynski, Nucl. Phys. A215, 91 (1973).
[2]V. V. Volkov, Phys. Rep. 44, 93 (1978).
[3]W. U. Schröder, J. R. Birkelund, J. R. Huizenga, K. L. Wolf, and V. E. Viola, Jr., Phys. Rep. 45, 301 (1978).
[4]M. Lefort and C. Ngô, Riv. Nuovo Cimento 2, No. 12 (1979).
[5]Y. Eyal, A. Gavron, I. Tserruya, Z. Fraenkel, Y. Eisen, S. Wald, R. Bass, G. R. Gould, G. Kreyling, R. Renfordt, K. Stelzer, R. Zitzmann, A. Gobbi, U. Lynen, H. Stelzer, I. Rode, and R. Bock, Phys. Rev. Lett. 41, 625 (1978).
[6]J. Péter, M. Berlanger, C. Ngô, B. Tamain, B. Lucas, C. Mazur, M. Ribrag, and C. Signarbieux, Z. Phys. A 283, 413 (1977).
[7]D. Hilscher, J. R. Birkelund, A. D. Hoover, W. U. Schröder, W. W. Wilcke, J. R. Huizenga, A. C. Mignerey, K. L. Wolf, H. F. Breuer, and V. E. Viola, Jr., Phys. Rev. C 20, 576 (1979).
[8]D. L. Hillis, O. Christensen, B. Fernardez, J. D. Garrett, G. B. Hagemann, B. Herskind, B. B. Back, and F. Folkmann, Phys. Lett. 78B, 405 (1978).
[9]L. Westerberg, D. G. Sarantites, D. C. Hensley, R. A. Dayras, M. L. Halbert, and J. H. Barker, Phys. Rev. C 18, 796 (1978).
[10]J. B. Ball, C. B. Fulmer, M. L. Mallory, and R. L. Robinson, Phys. Rev. Lett. 40, 1698 (1978).
[11]T. J. M. Symons, P. Doll, M. Bini, D. L. Hendrie, J. Mahoney, G. Mantzouranis, D. K. Scott, K. Van Bibber, Y. P. Viyogi, H. H. Wieman, and C. K. Gelbke, Lawrence Berkeley Laboratory Report No. LBL 8379 (1978).
[12]B. B. Back, Ole Hansen, H. C. Britt, and J. D. Garrett, Phys. Rev. C 9, 1924 (1974).
[13]W. J. Nicholson and I. Halpern, Phys. Rev. 116, 175

(1959).
[14]Torbjørn Sikkeland, Eldon L. Haines, and Victor E. Viola, Jr., Phys. Rev. 125, 150 (1962).
[15]P. Dyer, T. C. Awes, C. K. Gelbke, B. B. Back, A. Mignerey, K. L. Wolf, H. Breuer, and V. E. Viola, Jr., Phys. Rev. Lett. 42, 560 (1979).
[16]T. C. Awes, C. K. Gelbke, B. B. Back, A. C. Mignerey, K. L. Wolf, P. Dyer, H. Breuer, and V. E. Viola, Jr., Phys. Lett. 87B, 43 (1979).
[17]H. W. Schmitt, W. E. Kiker, and C. W. Williams, Phys. Rev. 137, B837 (1965).
[18]R. Vandenbosch and J. R. Huizenga, *Nuclear Fission* (Academic, New York, 1973), p. 339.
[19]J. E. Gindler, K. F. Flynn, L. E. Glendenin, and R. K. Sjoblom, Phys. Rev. C 16, 1483 (1977).
[20]C. K. Gelbke, C. Olmer, M. Buenerd, D. L. Hendrie, J. Mahoney, M. C. Mermaz, and D. K. Scott, Phys. Rep. 42, 311 (1978).
[21]C. K. Gelbke, D. K. Scott, M. Bini, D. L. Henrie, J. L. Laville, J. Mahoney, M. C. Mermaz, and C. Olmer, Phys. Lett. 70B, 415 (1977).
[22]A. S. Goldhaber, Phys. Lett. 53B, 306 (1974).
[23]K. W. McVoy and M. C. Nemes, Z. Phys. A 295, 177 (1980).
[24]T. Udagawa, T. Tamura, T. Shimoda, M. Fröhlich, M. Ishihara, and K. Nagatani, Phys. Rev. C 20, 1949 (1979).
[25]Y. Alhassid, R. D. Levine, J. S. Karp, and S. Steadman, Phys. Rev. C 20, 1789 (1979).
[26]F. Pühlhofer, Nucl. Phys. A280, 267 (1977).
[27]J. P. Bondorf, J. N. De, A. O. T. Karvinen, G. Fai, and B. Jacobsson, Phys. Lett. 84B, 162 (1979); J. P. Bondorf, J. N. De, G. Fai, A. O. T. Karvinen, B. Jacobsson, and J. Randrup, Nucl. Phys. A333, 285 (1980).
[28]K. Siwek-Wilczynska, E. H. du Marchie van Voorthuysen, J. van Popta, R. H. Siemssen, and J. Wilczynski, Phys. Rev. Lett. 42, 1599 (1979); Nucl. Phys. A330, 150 (1979).
[29]H. Yamada, D. R. Zolnowski, S. E. Cala, A. C. Kahler, J. Pierce, and T. T. Sugihara, Phys. Rev. Lett. 43, 605 (1979).
[30]G. D. Westfall, J. Gosset, P. J. Johansen, A. M. Poskanzer, W. G. Meyer, H. H. Gutbrod, A. Sandoval, and R. Stock, Phys. Rev. Lett. 37, 1202 (1976).
[31]L. J. Colby, Jr., Mary LaSalle Shoaf, and J. W. Cobble, Phys. Rev. 121, 1415 (1961).
[32]C. K. Gelbke, M. Bini, C. Olmer, D. L. Hendrie, J. L. Laville, J. Mahoney, M. C. Mermaz, D. K. Scott, and H. H. Wieman, Phys. Lett. 71B, 83 (1977).